Soft-switching Technique Applicable to Capacitive Load for Resonant Inverter of Plasma Generator

Koji Itakura, Hiroaki Kakemizu, Hiroki Nakaido,
Kazuhiro Umetani, Eiji Hiraki
Graduate School of Natural Science and Technology
Okayama University
Okayama, Japan

Tatsuya Ikenari and Shingo Kawano
Plasma System Division
DAIHEN Corporation
Osaka, Japan.

Published in: IECON 2017 - 43rd Annual Conference of the IEEE Industrial Electronics Society

DOI: 10.1109/IECON.2017.8216264

Soft-switching Technique Applicable to Capacitive Load for Resonant Inverter of Plasma Generator

Koji Itakura, Hiroaki Kakemizu, Hiroki Nakaido,
Kazuhiro Umetani, Eiji Hiraki
Graduate School of Natural Science and Technology
Okayama University
Okayama, Japan
umetani@okayama-u.ac.jp

Tatsuya Ikenari and Shingo Kawano
Plasma System Division
DAIHEN Corporation
Osaka, Japan.

***Abstract*—Recently, resonant inverters have been employed to generate high voltage high frequency AC power for plasma generator of the semiconductor processing equipment. This inverter is beneficial in low switching loss owing to its natural soft-switching capability under inductive load impedance. Generally, the resonant inverter for plasma generator is designed to have inductive load using an impedance matching circuit that interfaces the inverter and the plasma reactor. However, the load impedance often fluctuates according to the state of the plasma, momentarily causing the capacitive load impedance. In this case, the inverter is generally controlled to restrict the output power for circuit protection from excessive switching loss, although this will result in unstable plasma, deteriorating the quality of the semiconductor processing. This paper addressed this difficulty by applying a soft-switching technique to the resonant inverter. This soft-switching technique can be utilized regardless to the capacitive or inductive load. Experiment was carried out to evaluate the effectiveness of the proposed technique. As a result, the effective reduction of the switching loss was successfully verified even under the capacitive load impedance.**

Keywords—resonant inverter; soft-switching; capacitive load; plasma generator

I. INTRODUCTION

Plasma has been industrially utilized in the semiconductor manufacturing process. Plasma is commonly generated in the plasma reactor, in which high frequency large electric field is applied to the gas. In order to apply this electric field, the plasma reactor needs power supply with high frequency high AC voltage [1]–[4], as shown in the system diagram illustrated in Fig. 1.

Conventionally, linear amplifiers or vacuum tubes have been utilized for generating the required power supply. However, recent progress of the switching technology has given rises to the semiconductor switching inverters for power supply to the plasma reactor. Particularly, the resonant inverters are widely utilized as practical AC power supply [1]–[3].

The switching inverters for high frequency applications tend to suffer from enormous switching loss. Therefore, these inverters are intensely required to suppress the switching loss. The full-bridge resonant inverters [1]–[3][5]–[11], presented in Fig. 2, are known to be beneficial in suppressing the switching loss because it can naturally achieve soft-switching. Specifically, the full-bridge resonant inverters can achieve the zero-voltage turn-on and the zero-voltage turn-off under the inductive load impedance, although they cannot achieve soft-switching under the capacitive load impedance.

Therefore, the full-bridge resonant inverters for plasma generators require the equivalent impedance of the plasma reactor to be maintained inductive. In addition, impedance matching between the inverter and the plasma reactor is important particularly in high frequency application for effective power transfer to the plasma reactor. Therefore, an impedance matching circuit is generally added to interface the plasma reactor and the inverter.

The impedance matching circuit keeps the equivalent impedance of the plasma reactor to appear as an inductive load with the matched impedance to the inverter. However, small natural change of the state of the plasma may cause sudden fluctuation in the impedance of the plasma reactor. Certainly, the matching circuits are commonly designed to adjust itself automatically according to the impedance change of the plasma reactor. Nonetheless, the load impedance of the inverter, i.e. the equivalent impedance of the matching circuit and the plasma reactor, may momentarily appear as a capacitive and unmatched impedance, because the adjustment process of the impedance matching circuit is far slower than the switching period.

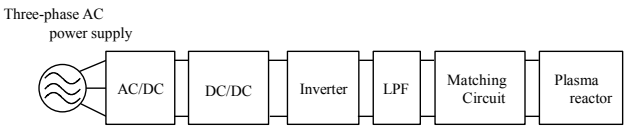

Fig. 1. Typical structure of the plasma generating system

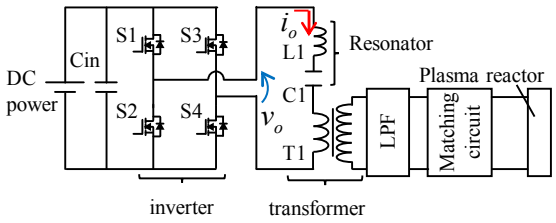

Fig. 2. Conventional full-bridge resonant inverter with the LPF, the matching circuit and the plasma reactor

In this condition, the inverter may be broken due to enormous switching loss resulted from incapability of the soft-switching. Otherwise, the inverter operation or the DC power supply to the inverter is stopped for protection of the inverter, resulting in insufficient generation of the plasma to deteriorate the quality of the semiconductor processing.

The purpose of this paper is to propose application of a soft-switching technique to the full-bridge resonant inverter to solve this issue. For this purpose, we focused on the previous soft-switching technique originally proposed for the PWM inverters [12]–[16]. This technique can achieve the zero-voltage turn-on and the zero-voltage turn-off regardless to the polarity or intensity of the output current. Therefore, this technique may also be effective for application to the full-bridge resonant inverter operating under the capacitive load impedance. Furthermore, this technique can be implemented by small additional circuit volume because the additional circuit carries the current only momentarily during the switching transition; and therefore heat generation at the additional circuit can be small.

The following discussion consists of three sections. Section II presents the proposed full-bridge resonant inverter as well as its operating principle. Section III presents the experiment to evaluate the operating principle and resultant loss reduction. Finally, section IV gives conclusions.

II. Proposed Inverter

A. Circuit Overview

Figure 3 illustrates the schematic diagram of the proposed resonant inverter. This proposed inverter incorporates the auxiliary circuit added to the conventional inverter, i.e. Fig. 2. (The auxiliary circuit is marked by the dashed box.) The auxiliary circuit mainly consists of inductor La and two switches Sa1 and Sa2.

Inductor La can have far smaller inductance than the main resonating inductor L1, as in the prototype presented in Section III. Therefore, a coreless inductor can be utilized for La, thus suppressing additional cost for La. In addition, switches Sa1 and Sa2 mainly carry the current only during the switching transition of the main switches S1–S4, as discussed in the next subsection. Therefore, Sa1 and Sa2 can be implemented by semiconductor switching devices with smaller current rating than S1–S4 because Sa1 and Sa2 do not tend to generate large conduction loss.

Besides, the auxiliary circuit incorporates a snubber circuit for Sa1 and Sa2, consisting of two snubber diodes Da1 and Da2. The snubber circuit is attached to dissipate the energy carried by the reverse recovery current of the body diodes of Sa1 and Sa2. Hence, the current of the snubber is generally far smaller than that of the main circuit; and therefore, the snubber circuit can be implemented by smaller circuit elements than the main circuit.

B. Operating Principle

This subsection discusses the operating principle of the proposed resonant inverter. As for the inductive load, the auxiliary switches Sa1 and Sa2 are always kept at the off-state. Therefore, no current flows in the auxiliary circuit; the operation of the proposed resonant inverter is the same as that of the conventional resonant inverter. Hence, the operation under the capacitive load impedance is discussed below.

Figure 4 shows the operating waveforms under the capacitive load impedance. Similarly as in the conventional full-bridge resonant inverter, S1 and S2 as well as S3 and S4 operate

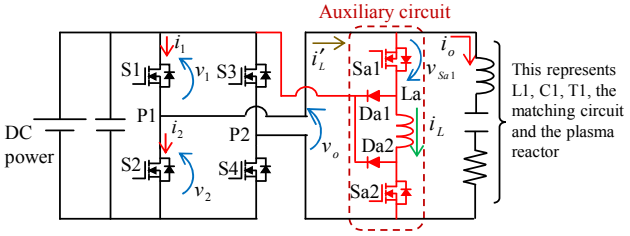

Fig. 3. Proposed full-bridge resonant inverter

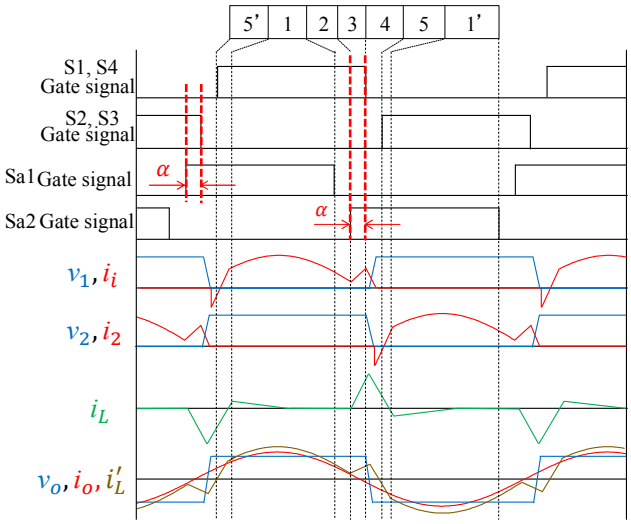

Fig. 4. Operating waveforms under the capacitive load. (Mode number with the prime indicates the modes in the next half switching period.)

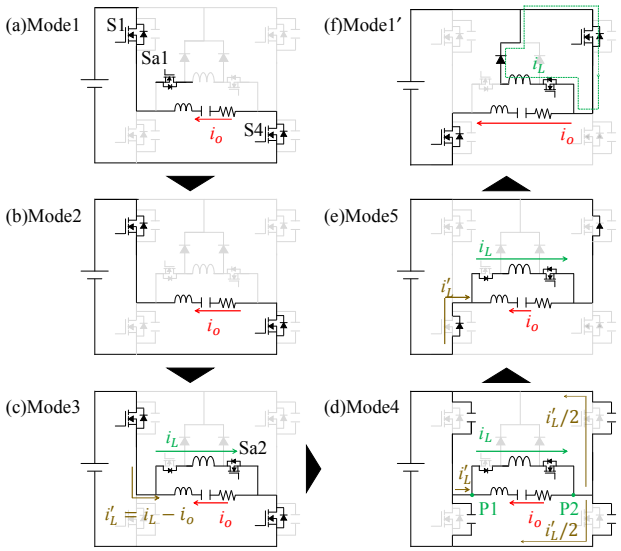

Fig. 5. Current pattern of the operating modes. (a) Mode1, (b) Mode2, (c) Mode 3, (d) Mode 4, (e) Mode 5, (f) Beginning of mode 1′ (circulation of the snubber current)

at the 180-degree phase-shift at the duty cycle of 0.5. In addition, Sa1 and Sa2 also operate at the 180-degree phase-shift at the duty cycle of 0.5. However, the phase of Sa1 slightly precedes that of S1. Because Sa1 and Sa2 as well as the main switches do not operate at a severe duty cycle close to zero or unity, the proposed resonant inverter can be operated at comparatively high switching frequency similarly as the conventional resonant inverter.

The operation of the first half of the switching cycle consist of 5 operating modes. The operation of the latter half is the same as that in the first half except that the current flows in the opposite direction; main switches S1, S2, S3, and S4 are replaced by S3, S4, S1, and S2, respectively; Sa1, Sa2, Da1, and Da2 are replaced by Sa2, Sa1, Da2, and Da1, respectively. Current patterns of each operating mode are presented in Fig. 5. In this figure, we express L1, C1, and T1, as well as the load, i.e. the LPF, the matching circuit, and the plasma reactor, as the equivalent LCR resonator to simplify the schematic diagram. (Hereafter, we refer to this equivalent resonator as the output resonator.) Below, operation of each mode is described.

Mode 1: Main switches S1 and S4 are kept at the on-state, whereas S2 and S3 are kept at the off-state to supply the positive voltage to the output resonator. Auxiliary switch Sa2 is in the off-state, whereas Sa1 is in the on-state. Because Sa2 is in the off-state, no current flows into the auxiliary circuit. Therefore, the operation is similar to that in the conventional resonating inverter.

Mode 2: Then, auxiliary switch Sa1 is turned off to make a dead time before the turn-on of Sa2. The turn-off of Sa1 is zero-voltage and zero-current transition.

Mode 3: After the dead time, auxiliary switch Sa2 is turned on. The current flows through the body diode of Sa1 to supply the current to auxiliary inductor La. The current of La increases linearly supplied with the DC voltage from the inverter. Because the current rise speed of Sa2 is restricted by La, Sa2 achieves the zero-current turn-on. After the current of La reaches above the current level of the output resonator flowing into the half bridge of S1 and S2, the operation steps into the next mode.

Mode 4: Main switches S1 and S4 are turned off, whereas S2 and S3 are still kept in the off-state to make the dead time. The duration of this dead time is generally short enough not to change the current of the output resonator and that of the auxiliary inductor La. Therefore, the current is flowing from point P1 toward point P2, as a result of summing the current of the output resonator and the auxiliary circuit. This current charges the drain-source stray capacitance of S1 and S4, and discharges that of S2 and S3. As a result, S1 and S4 achieves the zero-voltage turn-off. After charging and discharging the stray capacitance, the current from P1 to P2 flows through the body diode of S2 and S3.

Mode 5: Then, main switches S2 and S3 are turned on, whereas S1 and S4 are kept in the off-state. Because the current is still flowing through the body diode of S2 and S3, S2 and S3 achieve the zero-voltage turn-on. After the turn-on of S2 and S3, the current across La flows through the DC power supply, thus regenerating the magnetic energy stored in La. During the regeneration process, the current across La gradually decreases. After this current falls down to zero, the body diode of Sa1 is reverse biased to prevent the current flow into the auxiliary circuit. Certainly, the reverse recovery current may slightly flow through the body diode of Sa1. After the recovery of the body diode, this current forms a circulation loop through the snubber circuit, as shown in Fig. 5(f), thus gradually dissipating itself by the forward voltage drop of the snubber diode.

As we have seen above, all the semiconductor switches achieve soft-switching regardless to the inductive and capacitive load impedance: Main switches S1–S4 achieve the zero-voltage turn-on and the zero-voltage turn-off; auxiliary switches Sa1 and Sa2 achieve the zero-current turn-on and the zero-voltage turn-off. Therefore, the proposed resonant inverter is effective for switching loss suppression under both the inductive and capacitive load impedance.

C. Control of the Auxiliary Circuit

The only control required for the auxiliary circuit is the phase-shift between Sa1 and S2. Because the current across La should exceed the current of the output resonator at the end of mode 3, sufficient amount of the phase-shift, i.e. sufficient duration of mode 3, is needed. Nonetheless, excessively large phase-shift results in excessive conduction loss in the auxiliary circuit, which may deteriorate the efficiency improvement.

In this paper, we determined the phase-shift so that the parallel connection of the output resonator and the auxiliary circuit should have the inductive load impedance with the phase angle of $\pi/6$ rad. The required phase-shift time α, defined in Fig. 4, can be estimated as follows.

We regard the auxiliary circuit as a switched inductor circuit that equivalently works as the variable inductor with inductance L'_a. Note that auxiliary inductor La is equivalent to be directly connected in parallel to the load impedance at $\alpha=T/4$, where T is the switching period, and the peak of the La current is proportional to α, we can express $L'_a=L_aT/4\alpha$, where L_a is the inductance of La.

In the proposed inverter, the current waveform of the variable inductor is triangular because the square wave voltage is applied. On the other hand, the current waveform of the output resonator is sinusoidal excited by the fundamental wave of the square wave voltage. However, in order to simplify the discussion, both the output resonator (impedance R_0+jX_0) and the variable inductor are modeled to be excited by the fundamental wave of the square wave voltage output of the inverter as shown in Fig. 6.

Certainly, the equivalent inductance L_a'' of the variable inductor should be different from L_a' because L_a'' in this model

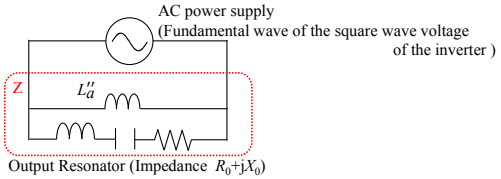

Fig. 6. Equivalent circuit model of the load (the LPF, the matching circuit and the plasma reactor) and the auxiliary circuit

TABLE I. SPECIFICATIONS OF PROTOTYPE OF PROPOSED INVERTER

Symbol	Parameter	Specification
	DC power supply	GPO350-20R, 350V, 20A
f	Switching frequency	400 kHz
	Forward power	1 kW
S1–S4	Main switch	APT5010JFLL, 500V, 41A
Cin	Input capacitors	EVS20329S2G306MS09, 30μF ×2
L1	Resonant inductance	17.45μH
C2	Resonant capacitance	ATC800E102, 1nF ×9
Sa1, Sa2	Auxiliary Switch	C2M0080120D, 1200V, 36A
Da1,Da2	Snubber diode	C4D40120D, 1200V, 54A
La	Auxiliary inductance	1.89μH

should have the same peak current as L_a' under the square wave voltage excitation. Noting that the peak current of an inductor induced by the fundamental wave of the square wave voltage is $8/\pi^2$ times as large as that that induced by this square wave voltage, we can express $L_a''=8L_a'/\pi^2$.

The total impedance Z of the parallel connection of the output resonator and the variable inductor L_a'' is obtained as follows, if we denote the angular frequency as ω:

$$Z=\frac{R_0\omega^2 L_a''^2}{R_0^2+\left(X_0+\omega L_a''\right)^2}+j\frac{\omega L_a''\left(R_0^2+X_0^2+\omega X_0 L_a''\right)}{R_0^2+\left(X_0+\omega L_a''\right)^2}. \quad (1)$$

Because Z should have the angle of π/6, α is determined as

$$\alpha=2L_a\left(R_0-2X_0\right)/\pi\left(R_0^2+X_0^2\right). \quad (2)$$

III. EXPERIMENT

An experiment was carried out to verify the operating principle as well as the power loss reduction by the proposed resonant inverter. In this experiment, prototypes of the proposed and conventional resonant inverters were designed and operated under the capacitive load impedance. The operating principle was evaluated by measuring the voltage and current waveforms of the prototypes. The power loss was evaluated by direct measurement of the efficiency. Besides, the loss breakdown was estimated to confirm that reduction in the power loss was contributed by reduction in the switching loss.

A. Experimetal Setup

Prototypes of the proposed and conventional resonant inverters have the same circuit diagrams as shown in Fig. 3 and Fig. 2, respectively. Specifications of the circuit elements are presented in Table I. These prototypes were designed to output maximum 2kW at 400kHz. The main switches and auxiliary switches are silicon MOSFETs (Si-MOSFETs) and silicon carbide MOSFETs (SiC-MOSFETs), respectively. SiC-MOSFETs can commonly achieve high speed switching compared with Si-MOSFETs. Therefore, SiC-MOSFETs are employed for the auxiliary switches to achieve exact turn-on timing for accurate phase shift time α.

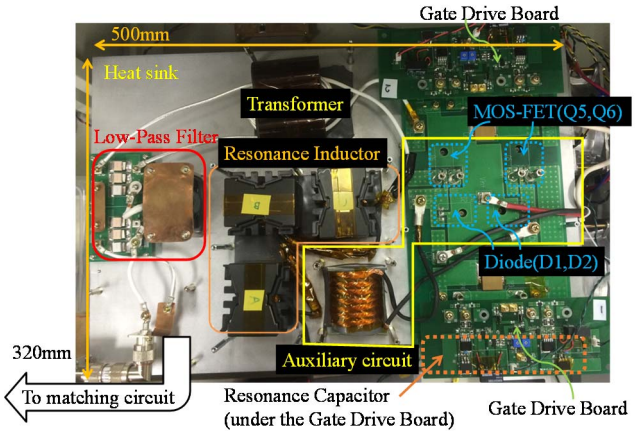

Fig. 7. Photograph of the prototype of the proposed inverter

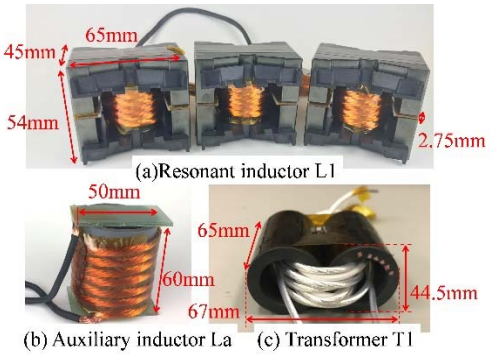

Fig. 8. Photographs of the magnetic devices of the prototypes

Figure 7 shows the photograph of the proposed resonant inverter. The main switches and the auxiliary switches have the ISO-TOP and TO-247 packages, respectively, mounted on the bottom side of the PCB to directly attach to the heat sink. As for the prototype of the conventional resonant inverter, we disconnected the auxiliary circuit from the prototype of the proposed inverter.

Figure 8 shows the photographs of resonant inductor L1, transformer T1, and auxiliary inductor La. L1 and T1 are both made of the Litz wire wound on the ferrite cores. On the other hand, La is made as a coreless coil of the Litz wire, because La was designed to have smaller inductance than L1. Specifications of the structures of these magnetic devices, including the core materials and the Litz wire, are presented in Table II.

Resonant inductor L1 is applied with high AC voltage. Therefore, L1 tends to suffer from large iron loss. In order to suppress the iron loss, L1 was composed as series-connected three inductors. By dividing the AC voltage among these inductors, the flux induction in each inductor core is reduced into 1/3 compared with L1 composed as a single inductor. Because the iron loss is approximately proportional to the square of the flux, the total iron loss of the series-connected three inductors can also be greatly reduced compared with L1 composed as a single inductor.

The inductance of La is determined to satisfy the requirement of the phase shift time α. The phase shift time α of

TABLE II. SPECIFICATIONS OF MAGNETIC DEVICES

Parameters	L1	La	T1
Magnetic core	PC95PQ65/54-Z ×3	-	H6FT44.5-13-30 ×10
Winding	600/2UEW 0.09mm		AF06B140SA
Turns	6T	7T	4T:8T
AC resistance (400kHz)	94mΩ	35.6mΩ	61mΩ (Primary equivalent resistance)
Self-inductance	17.45μH	1.89μH	–
Magnetizing inductance	-	-	143.6μH
Leakage inductance	-	-	0.653μH

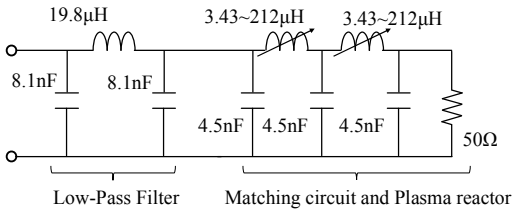

Fig. 9. Schematic diagram of the load for the prototypes

the proposed inverter was set after (2). Therefore, the value of α varies according to the load impedance. As discussed in subsection II.C, α cannot exceed $T/4$. As a result, too large inductance for La may result in insufficient soft-switching capability. According to (2), maximum allowable value of La can be obtained from $\alpha<T/4$ as

$$L_a < \pi\left(R_0^2 + X_0^2\right)T/8\left(R_0 - 2X_0\right). \quad (3)$$

In the prototype of the proposed inverter, La is determined to satisfy (3) at any load impedance tested in the experiment.

We tested the prototypes under the various capacitive load impedance for evaluation of the power loss. For this purpose, the load of the prototypes was designed to have adjustable load impedance. Figure 9 illustrates the schematic diagram of the load. The electric power applied to the load is dissipated by a 50Ω RF resistor (Bird Tech. 8329-300). However, the equivalent impedance of this resistor can be varied freely by adjusting the inductance of the two variable inductors.

B. Evaluation Result of Operating Waveforms

First, we evaluated the operating waveforms under the capacitive load impedance. In this experiment, the complex load impedance was set at 12.3–*j*6.8Ω. We operated the prototypes of the proposed and conventional resonant inverters with the forward power set at 1kW.

Figure 10 shows the voltage and current waveforms of the proposed resonant inverter during one switching period. Because of the symmetry between the two legs of the full-bridge, only the leg of S1 and S2 is observed. The measured waveforms were found to be consistent with those of the theoretical waveforms presented in Fig. 4. Certainly, the small La current (i_L) was found to flow in opposite direction throughout mode 1′ after the drop of this current in mode 5. This current is explained

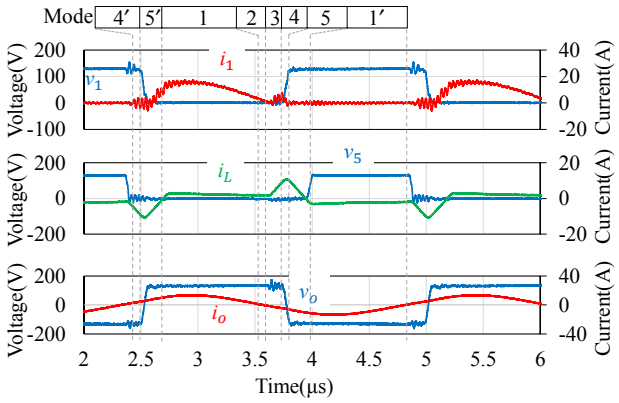

Fig. 10. Operating waveforms of the proposed resonant inverter

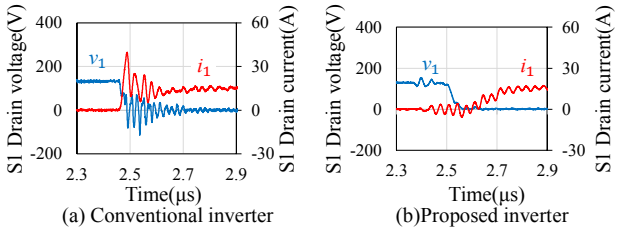

Fig. 11. Turn-on waveforms of the main switch S1

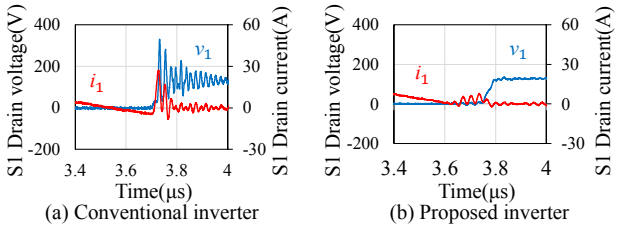

Fig. 12. Turn-off waveforms of the main switch S1

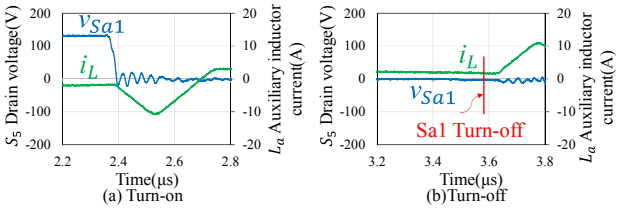

Fig. 13. Switching waveforms of the auxiliary switch Sa1

as the reverse recovery current of the body diode of the auxiliary switches forming the circulating current path through the snubber diodes. Therefore, the reverse recovery current was not entirely dissipated in the proposed circuit, although the remaining recovery current is far smaller than the peak of the La current.

Figure 11 and Fig. 12 show the comparison result of the turn-on and turn-off switching waveforms of main switch S1 between the proposed and conventional resonant inverters. As can be seen in the figure, the drain-source voltage dropped slightly before the turn-on of S1 in the proposed inverter, indicating the zero-voltage turn-on. Furthermore, the voltage rise was suppressed at the turn-off of S1 in the proposed inverter, indicating the zero-voltage turn-off. This result indicates that all

of the main switches achieve the zero-voltage turn-on and the zero-voltage turn-off because of the symmetry between S1 and S2 and the symmetry between the two legs.

Figure 13 shows the turn-on and turn-off switching waveforms of auxiliary switch Sa1. These waveforms indicate the zero-current turn-on, as is consistent with the theory. The turn-off waveforms were almost consistent with the zero-current zero-voltage turn-off, although slight current flows in the body diode of the auxiliary switch due to the remaining reverse recovery current circulating in the auxiliary circuit.

Consequently, the operating waveforms were found to support the operating principle.

C. *Evaluation Result of Power Loss*

Next, we compared the total power loss between the proposed and conventional resonant inverters. The power loss was evaluated under 11 capacitive load impedance. These evaluated lopad impedance are plotted on the Smith chart as shown in Fig. 14. These load impedance were chosen so that standing wave ratio (SWR) is kept below 4.0. The total power loss was evaluated by measuring the input power and the load power. The input power was measured using the power analyser (Yokogawa WT3000) connected in series between the DC power supply and the inverter. On the other hand, the load power is measured using the RF power meter (Bird Tech. 4027A and 4421) connected after the low-pass filter in Fig. 9.

Fig. 15 shows the measured power loss of the prototypes. The result indicates that the proposed resonant inverter successfully reduced the total power loss regardless to the load impedance. Certainly, this reduction effect was subtle at points A and B, where the capacitive reactance of the load impedance is comparatively small. In these points, the switching loss was small also in the conventional resonant inverter; and therefore, reduction of the switching loss by the proposed resonant inverter may be canceled by the conduction loss generated in the auxiliary circuit.

In order to investigate the contributor of this reduction effect of the total power loss, we estimated the loss breakdown at the load impedance of 12.3−j6.8Ω. (This load impedance corresponds to point I marked by the star in Fig. 14.) Conduction loss of the switches S1–S4, Sa1, Sa2 were estimated using the on-resistance data reported by the datasheet, whereas that of the diodes were estimated using the forward voltage drop data reported by the datasheet. Switching loss of the semiconductor switches were calculated based on the switching waveforms observed at this load impedance. Furthermore, the power loss of T1, L1, La, and LPF were estimated based on their AC resistance measured using the LCZ meter (NF Electronic Instruments 2340).

The result is shown in Fig. 16. As can be seen in the figure, the main contributor of the power loss reduction was found to be the switching loss, as is expected from the theory. Consequently, this experiment was found to support the effectiveness of the proposed resonant inverter.

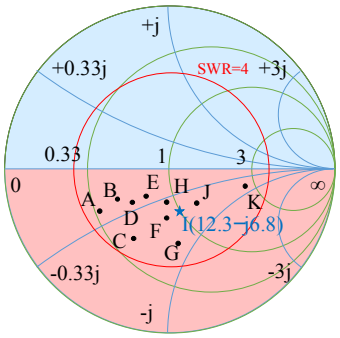

Fig. 14. Experimental load imedance (plotted on the Smith chart)

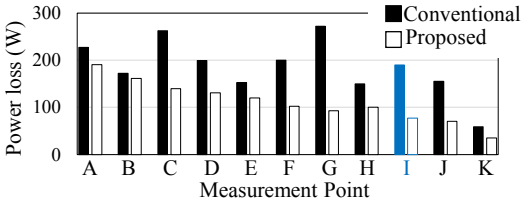

Fig. 15. Experimental result of the power loss

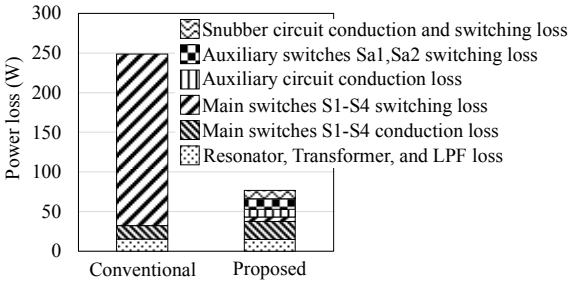

Fig. 16. Breakdown of total loss at point I

IV. Conclusions

Resonant inverters are widely utilized for the AC voltage supply of the plasma generator for the semiconductor processing equipment. Resonant inverters are effective for low power loss under the inductive load impedance owing to its natural soft-switching capability. However, sudden change of the state of the plasma may result in fluctuations of the load impedance, momentarily causing the capacitive load impedance. In this condition, the resonant inverter may suffer from large switching loss due to its soft-switching incapability under the capacitive load impedance.

In order to address this issue, this paper proposed a soft-switching technique applicable to the full-bridge resonant inverter. The proposed resonant inverter incorporates the auxiliary circuit added to the conventional resonant inverter. The experiment verified the soft-switching capability of the proposed inverter under the capacitive load impedance as well as the total power loss reduction owing to reduction in the switching loss.

V. Acknoeledgent

This work was supported by IEEJ Chugoku branch.

REFERENCES

[1] H. Fujita and H. Akagi, "A 2-MHz 2-kW voltage-source inverter for low-temperature plasma generators: implementation of fast switching with a third-order resonant circuit," IEEE Trans. Ind. Appl., vol. 35, no. 1, pp. 21–27, Jan./Feb. 1999.

[2] H. Fujita, H. Akagi, and S. Shinohara, "A 2-MHz 6-kVA voltage-source inverter using low-profile MOSFET modules for low-temperature plasma generators," IEEE Trans. Power Electron., vol. 14, no. 6, pp. 1014–1020, Nov. 1999.

[3] Y. Kim, J. Kim, S. Mun, H. Lee, S. Kwon, K. Suh, "The design of inverter power system for plasma generator," in Proc. Intl. Conf. Elect. Mach. Syst. (ICEMS2005), Nanjing, China, Sept., 2005, pp. 1309–1312.

[4] M. Balcerak, M. Holub, S. Kalisiak, M. Zenczak, "Topology of a high voltage pulse generator using parasitic parameters of autotransformers for non-thermal plasma generation," in Proc. Intl. Power Electron. Motion Ctrl. Conf. (EPE-PEMC2012), Novi Sad, Serbia, Sept., 2012, pp. DS1b.16-1–DS1b.16-6.

[5] M. K. Kazimierczuk and M. K. Jutty, "Fixed-frequency phase-controlled full-bridge resonant converter with a series load," IEEE Trans. Power Electron., vol. 10, no. 1, pp. 9–18, Jan. 1995.

[6] J. M. Burdio, L. A. Barragan, F. Monterde, D. Navarro, and J. Acero, "Asymmetrical voltage-cancellation control for full-bridge series resonant inverters," IEEE Trans. Power Electron., vol. 19, no. 2, pp. 461–469, Mar. 2004.

[7] C. Lin, "The design and implementation of a new digital dimming controller for the backlight resonant inverter," IEEE Trans. Power Electron., vol. 20, no. 5, pp. 1459–1466, Nov. 2005.

[8] V. Esteve, J. Jordan, E. Sanchis-Kilders, E. J. Dede, E. Maset, J. B. Ejea, and A. Ferreres, "Improving the reliability of series resonant inverters for induction heating applications," IEEE Trans. Ind. Electron., vol. 61, no. 5, pp. 2564–2572, May 2014.

[9] B. Esteban, M. Sid-Ahmed, and N. C. Kar, "A comparative study of power supply architectures in wireless EV charging systems," IEEE Trans. Power Electron., vol. 30, no. 11, pp. 6408–6422, Nov. 2015.

[10] J. Hu, C. Bi, K. Jia, and Y. Xiang, "Power control of asymmetrical frequency modulation in a full-bridge series resonant inverter," IEEE Trans. Power Electron., vol. 30, no. 12, pp. 7051–7059, Dec. 2015.

[11] B. Meziane and H. Zeroug, "Comprehensive power control performance investigations of resonant inverter for induction metal surface hardening," IEEE Trans. Ind. Electron., vol. 63, no. 10, pp. 6086–6096, Oct. 2016.

[12] J. S. Lai, R. W. Young, Sr., G. W. Otta, Jr., and D. Chen, "A novel resonant snubber based soft-switching inverter," in Proc. IEEE Appl. Power Electron. Conf. Expo. (APEC1995), Dallas, TX, USA, Mar., 1995, pp. 797–803.

[13] H. Zhu, J. Lai, A. R. Hefner, Jr., Y. Tang, and C. Chen, "Modeling-based examination of conducted EMI emissions from hard- and soft-switching PWM inverters," IEEE Trans. Ind. Appl., vol. 37, no. 5, pp. 1383–1393, Sept./Oct. 2001.

[14] H. Takano, T. Domoto, J. Takahashi, and M. Nakaoka, "Auxiliary resonant commutated soft-switching inverter with bidirectional active switches and voltage clamping diodes," in Proc. IEEE Ind. Appl. Conf., Chicago, IL, USA, Oct., 2001, pp. 1441–1446.

[15] N. Hoshi and S. Nagata, "Dead-time compensation scheme for adjustable dead-time controlled resonant snubber inverter," in Proc. IEEE Intl. Power Electron. Motion Ctrl. Conf. (IPEMC2009), Wuhan, China, May, 2009, pp. 1508–1513.

[16] R. Born, L. Zhang, Y. We, Q. Ma, J. Lai, "Interleaved auxiliary resonant snubber for high-power, high-density applications," in Proc. IEEE Energy Conversion Conf. Expo. (ECCE2016), Milwaukee, WI, USA, Sept., 2016, pp. 1–6.